

The Balmer decrement of SDSS galaxies

Brent Groves^{★1,2}, Jarle Brinchmann¹, and Carl Jakob Walcher³

¹*Leiden Observatory, Leiden University, P.O. Box 9513, 2300 RA Leiden, The Netherlands*

²*Max Planck Institute for Astronomy, Königstuhl 17, D-69117 Heidelberg, Germany*

³*Astrophysikalisches Institut Potsdam, An der Sternwarte 16, D-14482 Potsdam, Germany*

25 February 2024

ABSTRACT

High resolution spectra are necessary to distinguish and correctly measure the Balmer emission lines due to the presence of strong metal and Balmer absorption features in the stellar continuum. This accurate measurement is necessary for use in emission line diagnostics, such as the Balmer decrement (i.e. $H\alpha/H\beta$), used to determine the attenuation of galaxies. Yet at high redshifts obtaining such spectra becomes costly. Balmer emission line equivalent widths are much easier to measure, requiring only low resolution spectra or even simple narrow band filters and therefore shorter observation times. However a correction for the stellar continuum is still needed for this equivalent width Balmer decrement. We present here a statistical analysis of the Sloan Digital Sky Survey Data Release 7 emission line galaxy sample, using the spectrally determined Balmer emission line fluxes and equivalent widths. Using the large numbers of galaxies available in the SDSS catalogue, we determined an equivalent width Balmer decrement including a statistically-based correction for the stellar continuum. Based on this formula, the attenuation of galaxies can now be obtained from low spectral resolution observations. In addition, this investigation also revealed an error in the $H\beta$ line fluxes, within the SDSS DR7 MPA/JHU catalogue, with the equivalent widths underestimated by average $\sim 0.35\text{\AA}$ in the emission line galaxy sample. This error means that Balmer decrement determined attenuations are overestimated by a systematic 0.1 magnitudes in A_V , and future analyses of this sample need to include this correction.

Key words: galaxies: starburst – galaxies: statistics – galaxies: active – dust, extinction

1 INTRODUCTION

The Balmer lines are the most well known and observed emission lines in astronomy, being both strong lines in the optical and ubiquitous as they arise from recombination to the $n = 2$ level of the most common element, hydrogen. As the atomic structure of hydrogen is so well understood, the strength of the emission line fluxes can be well determined if the radiation field ionizing the hydrogen gas is known, and, importantly, the relative fluxes of the resulting hydrogen emission lines are only weakly dependent on the local conditions. Given that the ratios are well determined, the difference between the measured ratios of the Balmer lines and the intrinsic values expected can be used to determine the reddening of galaxies, or, more accurately, the ionized regions within them. In association with an attenuation/reddening-law and selective-to-total attenuation, R_V , the reddening can then give the total attenuation of a galaxy (e.g. the oft used work of Calzetti 2001). This possibility of using the hydrogen emission lines, in particular the ratio of the two strongest Balmer lines $H\alpha$ and $H\beta$, to measure the reddening and attenuation has been known and utilized for many years (e.g. Berman

1936, was one of the first mentions of the Balmer decrement being affected by the path length through an absorbing medium).

However, the accurate measurement of the Balmer decrement (i.e. the ratio of $H\alpha/H\beta$) requires the measurement of both the relatively weak $H\beta$ line and the continuum underneath it to distinguish the line. Separation of the underlying continuum from the Balmer emission lines is vital as the metal absorption lines and, especially, Balmer absorption lines present in the spectrum of later-type stars act to weaken or hide the relative flux of the emission lines in the integrated spectra of galaxies. Such was shown by Liang et al. (2004), where the $H\beta$ line was not observed in a selection of galaxies in low-resolution spectra ($R = 150$) from the the Canada-France-Redshift Survey, but moderate resolution spectra ($R > 600$) revealed the weak $H\beta$ lines hidden by both dust and absorption lines. The exposure times needed to obtain sufficient spectral resolution to distinguish the emission lines from the underlying stellar continuum of galaxies means that studies of the Balmer decrement tend to be biased to high emission-line equivalent width objects. While this bias may not be a serious issue, with dustier, more attenuated objects tending to have higher specific star formation rates and thus higher emission line equivalent widths (see e.g. da Cunha et al. 2010), such biases do tend to limit samples for

★ brent@mpia.de

investigations of dust and star formation. This is especially so at higher redshifts where the high spectral resolution needed to resolve both the line and continuum limits surveys to the brightest objects.

Even with moderate resolution spectra, the Balmer emission line fluxes are still sensitive to the way the stellar absorption is accounted for, and this can be a substantial source of error, particularly for weak emission line sources.

It is these issues that motivates us to examine the possibility of determining the decrement from the *equivalent widths* of the Balmer emission lines. Emission line equivalent widths do not require high resolution spectra to distinguish the line from the continuum, allowing the use of low resolution spectra, such as at $R \sim 300$, enabling fainter objects or more objects to be observed for the same exposure time as high resolution spectra. Even at only $R \sim 100$, as will be available with the multi-object *NIRSpec* on JWST, the influence of $H\beta$ on the interpretation of galaxy spectra can still be significant (Pacifi et al., in prep), and the line is still detectable at a signal-to-noise ~ 5 for some of the brighter emission-line galaxies. The issue at these low resolutions (i.e. $R < 300$) becomes one of distinguishing individual lines, such as $[\text{N II}]\lambda 6584\text{\AA}$ from $H\alpha$, not detecting the lines.

To examine how the Balmer line equivalent widths can be used to determine the Balmer decrement we use the Sloan Digital Sky Survey (SDSS Abazajian et al. 2009), which contains a large spectroscopic sample of emission line galaxies covering a wide range of galaxy types and properties, including attenuations. With such a wide range of galaxies, and reasonably high resolution spectra ($R \sim 1900$), the SDSS provides the perfect sample for examining this issue. With the large number of SDSS galaxies it is possible to obtain a statistically representative estimate for the correction factors needed (i.e. the Balmer absorption lines) and thus determine the Balmer decrement from equivalent widths alone.

This method should be seen as complementary to the stellar spectral synthesis continuum fitting methods widely used in the analysis of galaxy spectra. Codes such as PLATEFIT (Tremonti et al. 2004, used for the determination of the stellar properties in the SDSS MPA/JHU catalogue used here) and (Lamareille et al. 2006, applied this to lower resolution, higher redshift data in the VVDS sample), pPXF (Cappellari & Emsellem 2004), STARLIGHT (Cid Fernandes et al. 2005), STECKMAP (Ocvirk et al. 2006), and VESPA (Tojeiro et al. 2007), all use linear combinations of synthetic stellar population spectra (such as from Bruzual & Charlot 2003) to fit the full observed spectra of galaxies using various optimized maximum likelihood approaches. These codes have been created to extract the maximum possible information from galaxy spectra given degeneracies and noise (see e.g. the discussion in Ocvirk et al. 2006), and thus are clearly the best approach when strong continuum is detected. Yet the amount of possible information to be extracted reduces with both decreasing signal-to-noise ratio and spectral resolution. In addition, these methods are limited by the available spectral libraries, which may not cover the full parameter range needed to match the observed galaxies, and may have intrinsic issues, as we demonstrate here in an issue we discovered in the course of this paper. Thus an empirical method as we explore here is fully complementary to the spectral synthesis methods used in most works.

In the following sections we introduce the Balmer lines, both in absorption and emission (§2), the SDSS emission-line galaxy sample (§3, provide a possible way to determine the Balmer decrement from the equivalent widths (§4), and finally also point out an

	λ (Å)	5000K	10,000K	20,000 K
$H\alpha$	6562.80	3.04	2.86	2.75
$H\beta$	4861.32	1.00	1.00	1.00
$H\gamma$	4340.46	0.458	0.468	0.475
$H\delta$	4101.73	0.251	0.259	0.264

Table 1. Balmer lines, including rest-frame wavelengths (Air), and their ratios relative to $H\beta$ for $n_e = 10^2 \text{ cm}^{-3}$ and 3 different temperatures ([values from Dopita & Sutherland (2003), based on data from Storey & Hummer (1995)).

interesting problem with the fitting of the stellar continuum in the SDSS (§2).

2 THE BALMER LINES AND DECREMENT

2.1 Balmer emission lines

The Balmer emission lines in the interstellar medium arise predominantly from the recombination and subsequent cascade of electrons to the $n = 2$ level of hydrogen. While collisional excitation can also contribute to the Balmer line emission in hot media (see e.g. Ferland et al. 2009), photoionization and recombination are the predominant energetic processes in most galaxies.

As the atomic structure of hydrogen is so simple, it is possible to determine the exact electronic transition rates, and therefore the ratios of resulting emission lines from these transitions, as a function of physical conditions in the interstellar medium (see Menzel & Baker (1937); Baker & Menzel (1938) for the original theory, with updated work by Seaton (1959) and Storey & Hummer (1995), and treatments of this theory found in textbooks such as Osterbrock & Ferland (2006) or Dopita & Sutherland (2003)). In particular, two cases exist for which the Balmer decrement has been determined over a range of temperatures and densities: Case A and Case B. Case A assumes that an ionized nebula is optically thin to all Lyman emission lines (i.e. lines emitted from transitions to the $n = 1$ level of hydrogen), while Case B assumes that a nebula is optically thick to all Lyman lines greater than $\text{Ly}\alpha$ (i.e. transitions to $n = 1$ from levels $n = 3$ and above), meaning these photons are absorbed and re-emitted as a combination of $\text{Ly}\alpha$ and higher order lines, such as the Balmer lines. These two cases will lead to different intrinsic ratios for the Balmer lines, with variations of the same order as temperature effects (for other possible “Cases” of emission which may occur, see e.g. Ferland 1999; Luridiana et al. 2009). While Case B is typically assumed for determining intrinsic ratios, in reality the ratio in typical H II regions lies between these two cases, and must be determined using radiative transfer codes such as MAPPINGS III (see eg Groves et al. 2004) or CLOUDY (Ferland et al. 1998).

In Table 1 we present the four strongest Balmer emission lines and their ratios relative to $H\beta$ assuming Case B conditions. These ratios are only weakly sensitive to density, with the $H\alpha/H\beta$ ratio at $T = 10^4 \text{ K}$ equal to 2.86, 2.85, and 2.81 for the electron densities $n_e = 10^2$, 10^4 , and 10^6 cm^{-3} respectively, hence we only show the larger variation due to temperature here. For a full ratio description see Table B.7 in Dopita & Sutherland (2003), or Table 4.4 in Osterbrock & Ferland (2006). While these variations due to temperature and density are significant, they are still small relative to the effects of dust, as visible in the later sections, and hence strong diagnostics for the amount of reddening experienced by an emission line galaxy.

2.2 Balmer absorption lines

As discussed in the introduction, the fitting of the underlying stellar continuum is a vital step in determining line fluxes, especially for hydrogen (e.g. Balmer) and helium recombination lines, which have underlying corresponding absorption lines. The Balmer absorption lines arise from the absorption of light by hydrogen in the excited $n = 2$ level in the photospheres of stars. The strength of the absorption is dependent on both the effective temperature and gravity, as they require a significant fraction of hydrogen to be excited to the $n = 2$ level (see e.g., Table 4 in González Delgado & Leitherer 1999). The maximum equivalent widths occur around $T_{\text{eff}} \sim 9000\text{K}$, corresponding to early A-type stars.

For a simple, single-aged stellar population, the equivalent widths (EW) of the Balmer stellar absorption features depend on the age and, more weakly, on the metallicity, and vary from $\sim 2\text{\AA}$ to $\sim 15\text{\AA}$ with the maximum value occurring for stars aged around 500 Myr (i.e. dominated by the light from A & F stars). In Figure 1 we show the variation of the equivalent widths (EW) respectively for simple stellar populations as a function of age and metallicity (as labelled in the left hand of the figure in the $H\delta$ diagrams). We compare the four strongest lines; $H\alpha$, $H\beta$, $H\gamma$, and $H\delta$, using four models to determine the equivalent widths as labelled in the upper right; the Bruzual & Charlot (2003, BC03) stellar population synthesis code using the MILES (Sánchez-Blázquez et al. 2006; Cenarro et al. 2007) and Stelib (Le Borgne et al. 2003) stellar spectral libraries, and the 2008 version of the Charlot & Bruzual (in prep, CB08) code with the MILES library. Also shown by the dashed lines are the results from González Delgado & Leitherer (1999). The weak dependence on metallicity and the strong dependence on age, with the peak in EW at 0.5 – 1 Gyr for all lines, are clearly seen for all models. The equivalent widths are reasonably similar between the dominant Balmer lines (i.e. $H\alpha$, $H\beta$, $H\gamma$, and $H\delta$) varying at most a factor of ~ 2 (Kauffmann et al. 2003a; González Delgado & Leitherer 1999; González Delgado et al. 1999).

Thus, as the equivalent widths of the stellar absorption features are approximately constant with wavelength while the relative strength of the Balmer emission lines decrease rapidly with decreasing wavelength (i.e. for the higher order lines), stellar absorption affects strongly the measurement of the Balmer decrement i.e. $H\alpha/H\beta$, $H\gamma/H\delta$. This is especially so for weak emission line galaxies where the stellar absorption features are relatively stronger and only $H\alpha$ is seen in emission. This relative importance of the effect of the stellar Balmer absorption on the emission lines is important when considering the Balmer ratios, as discussed in later sections.

3 THE SDSS SAMPLE

Within this work we base our findings on the spectroscopic data from the seventh Data Release of the SDSS (DR7 Abazajian et al. 2009), though we also refer to the fourth Data Release (DR4 Adelman-McCarthy et al. 2006) as well when necessary. The SDSS used a pair of multi-fibre spectrographs with fibres of $3''$ diameter. In most galaxies the fibres were placed as close as possible to the centres of the target galaxies. The flux- and wavelength-calibrated spectra cover the range from 3800 to 9200 \AA , with a resolution of $R \sim 1900$.

We obtain our emission line fluxes from the MPA/JHU analy-

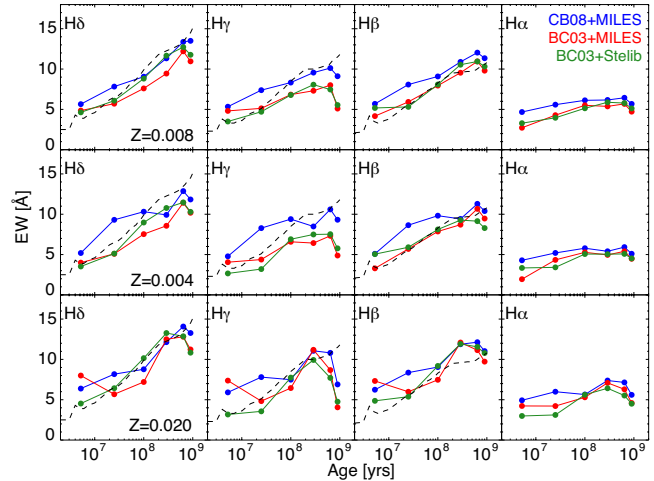


Figure 1. Equivalent widths (EW) of the four dominant Balmer lines, $H\alpha$, $H\beta$, $H\gamma$, and $H\delta$ (as labelled), for simple stellar populations of varying age and metallicity (increasing from top to bottom row, as marked on lower left in $H\delta$ figure). Three stellar synthesis models are considered, as indicated by the colours in the key in the upper right; the Bruzual & Charlot (2003, BC03) stellar population synthesis code using the MILES (Sánchez-Blázquez et al. 2006; Cenarro et al. 2007) and Stelib (Le Borgne et al. 2003) stellar spectral libraries, and the 2008 version of the Charlot & Bruzual (in prep, CB08) code with the MILES library. The dashed line shows the results from González Delgado & Leitherer (1999).

sis of the SDSS spectroscopic sample¹. This database contains, in addition to the emission line fluxes, derived physical properties for all spectroscopically observed galaxies in the SDSS DR7. The procedure for emission line measurement, detailed in Tremonti et al. (2004), was to correct the line fluxes for stellar absorption, fitting a non-negative combination of stellar population synthesis models from Charlot & Bruzual (in prep., CB08)² for the SDSS DR7 release and Bruzual & Charlot (2003, BC03) for the SDSS DR4 release³. The best-fitting stellar population model also places constraints on the star formation history and metallicity of the galaxy (see e.g. Gallazzi et al. 2005), and has been used to estimate stellar masses and star-formation histories (Kauffmann et al. 2003a).

The equivalent widths of the Balmer lines we use here, also available as part of the MPA/JHU database (listed as (line name)_reqw in the gal_line data file), are computed from straight integration over the continuum-subtracted bandpasses listed in table 2. Note that, by definition, emission lines have negative values of equivalent width but for clarity in the rest of the paper we assign all emission lines a positive value. The continuum in this case is estimated using a running median with a 200 pixel window and does not properly account for stellar absorption. This measurement is representative of the cases where a more accurate determination of the stellar continuum, as done with the MPA/JHU database, is not

¹ The data catalogues are available from <http://www.mpa-garching.mpg.de/SDSS/>

² The model spectra used were from an early version of the models and differ from what will be eventually published. The differences from BC03 are primarily due to different treatment of TP-AGB stars and that the empirical stellar library used was the MILES library rather than STELIB.

³ The spectra are available as part of the GALAXEV package, which can be obtained from <http://www2.iap.fr/users/charlot/bc2003/index.html>.

Table 2. Equivalent width bandpass

Line	Centre (Å)	Lower bound (Å)	Upper bound (Å)
H δ	4101.73	4092.0	4111.0
H γ	4340.46	4330.0	4350.0
H β	4861.32	4851.0	4871.0
H α	6562.80	6553.0	6573.0

possible, such as with low resolution or low S/N data, and helps characterize the effects of stellar absorption on the lines.

As we concentrate on emission line galaxies in this work, in particular galaxies with measurable Balmer emission lines, we have placed cuts on the signal-to-noise (S/N) of the Balmer emission lines using the uncertainties given by the MPA/JHU catalogue. As discussed on the website, the listed uncertainties are formal, and likely underestimates, thus we increase the uncertainty estimates on the emission lines to take into account continuum subtraction uncertainties by the factors listed on the web site determined by comparisons of duplicate observations within the SDSS sample. Specifically for the Balmer lines, we multiply the line flux uncertainty estimates by a factor of 1.882. From the full SDSS emission line galaxy sample we define three galaxy samples depending on the lines and ratios being examined; $\text{SN}(\text{H}\alpha, \text{H}\beta)$, $\text{SN}(\text{H}\alpha, \text{H}\beta, \text{H}\gamma)$, and $\text{SN}(\text{H}\alpha, \text{H}\beta, \text{H}\gamma, \text{H}\delta)$, where we require a $\text{S/N} > 3$ in two or more of the four strongest Balmer lines (H α , H β , H γ , & H δ). The S/N cuts are dominated by the weakest line in each sample due to the strong decrease in relative flux for the higher order lines, thus the inclusion of each higher order line biases the samples to higher equivalent widths of the H α emission line. As shown in figure 2, beginning from the full galaxy sample of SDSS DR7 ($\sim 928,000$ galaxies), approximately half are emission line galaxies ($\sim 510,000$, as measured by the presence of H α in emission), with a broad spread of equivalent widths peaking at $\sim 20\text{\AA}$ (as measured from the local continuum, not corrected for stellar absorption). As each higher order Balmer line is included, the sample rapidly decreases and is biased to higher equivalent widths, with the $\text{SN}(\text{H}\alpha, \text{H}\beta, \text{H}\gamma, \text{H}\delta)$ sample limited to $\sim 120,000$ galaxies with $\text{EW}(\text{H}\alpha) > 10\text{\AA}$, with a distribution peaking at 32\AA ($\text{SN}(\text{H}\alpha, \text{H}\beta)$ has $\sim 392,000$ galaxies, while $\text{SN}(\text{H}\alpha, \text{H}\beta, \text{H}\gamma)$ has $\sim 241,000$ galaxies). As the emission line $\text{EW}(\text{H}\alpha)$ in a galaxy spectrum can be considered a proxy for the specific star formation rate (the current star formation rate relative to the total stellar mass, $\text{sSFR} = \text{SFR}/M_*$) of a galaxy, the bias in $\text{EW}(\text{H}\alpha)$ means a bias to more “starforming” galaxies, which means a bias to lower-mass, lower-metallicity, bluer galaxies as shown in previous works (Brinchmann et al. 2004; Tremonti et al. 2004). This bias needs to be kept in mind when considering the diagrams and analysis in this work.

Figure 2 also reveals the limitation of low-resolution spectroscopy in finding all emission line sources, and thus the limitation of applicability of the method we explore here. Approximately 5% of the $\text{SN}(\text{H}\alpha)$ sample, and even 0.7% of the $\text{SN}(\text{H}\alpha, \text{H}\beta)$ sample, actually have $\text{EW}(\text{H}\alpha)$ less than zero (i.e. the emission line is lost in the stellar absorption feature). These sources would never be picked up as emission line galaxies in low-resolution spectra, and the use of an emission-line equivalent width Balmer decrement to determine the attenuation would return spurious results.

Note that we have not included any cuts on redshift or the type of emission-line galaxy as in previous works on SDSS emission line galaxies (e.g. Kewley et al. 2006). Such redshift cuts are necessary to make certain that aperture effects do not play a part

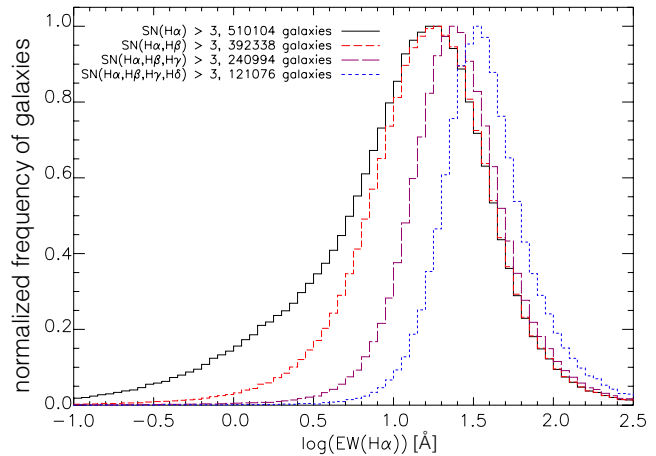


Figure 2. Distribution of the H α emission line equivalent widths for the samples considered in this work. All four histograms are normalized to their peak value, with the total number of galaxies in each sample listed in the key in the upper left. The solid histogram shows all emission line galaxies in SDSS DR7 (defined by the presence of H α in emission), and the three dashed curves show the distributions of samples defined by S/N cuts in the Balmer lines (as labelled in the upper left) considered in this work.

in the derived galaxy properties (by sampling only a small, biased part of the galaxy, as discussed in Kewley et al. 2005) and to prevent luminosity biases at the higher redshifts. Yet as we care only for the derived Balmer emission line fluxes and stellar equivalent widths these issues do not strongly affect our findings.

Separating emission-line galaxies by class (i.e. star-forming or Active Galactic Nucleus dominated) is necessary when examining the structure of the forbidden emission lines (e.g. [O III] $\lambda 5007\text{\AA}$) which depend strongly on the dominant ionization mechanism in the gas (see e.g. Kewley et al. 2006), and when comparing physical galaxy properties with emission line properties (see e.g. Kauffmann et al. 2003a,b). However, as discussed in the previous section, the relative strength of the Balmer lines depend only weakly on local conditions, and will vary little in their intrinsic ratios between being photoionized by AGN or by OB stars (i.e. H α /H β should be ~ 2.86 in star-forming galaxies and ~ 3.1 in galaxies ionized purely by an AGN). Thus, while this difference is significant and will have some bearing on the work in this paper, it is secondary to the effects of dust attenuation. Only when collisional heating dominates the atomic gas and the excitation of hydrogen, such as in shocks or clouds in hot gas, can the intrinsic ratios be significantly different (see e.g. Ferland et al. 2009), but these processes are not expected to dominate most galaxies within our sample. An additional reason to include AGN is that, in accordance with our main aim, separating out the contribution of AGN from lower S/N samples may prove problematic as the weak diagnostic lines become lost within the noise.

Approximately 2% of the full SDSS sample considered here are duplicate observations of galaxies (i.e. $\sim 4\%$ of the sample are pairs). We have not removed these from the sample so as to include the intrinsic scatter due to observational uncertainties in the subsequent analysis.

4 THE EQUIVALENT WIDTH BALMER DECREMENT

The issue of simply using directly the equivalent widths of the Balmer lines as proxies for the line fluxes when calcu-

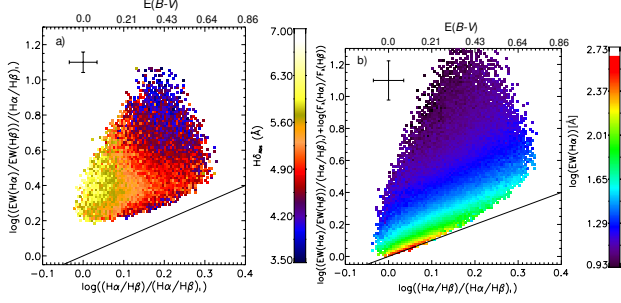


Figure 3. The variation of the equivalent width based Balmer decrement ($\log[\text{EW}(\text{H}\alpha)/\text{EW}(\text{H}\beta)]$) versus the stellar continuum-subtracted flux based Balmer decrement for the SDSS SN($\text{H}\alpha, \text{H}\beta$) sample. All axes are normalized by the intrinsic Balmer ratio, $(\text{H}\alpha/\text{H}\beta)_I = 2.86$. In the left diagram, the $\text{EW}(\text{H}\alpha/\text{H}\beta)$ has not been corrected for the difference in continuum flux at the $\text{H}\alpha$ and $\text{H}\beta$ wavelengths ($F_\lambda(\text{H}\alpha)/F_\lambda(\text{H}\beta)$), while in the right this is included. The upper left hand corner shows the median uncertainties for the sample, and the straight line indicates a 1:1 relation. The colours and associated colourbars indicate the median $\text{H}\delta_{\text{Abs}}$ and $\log[\text{EW}(\text{H}\alpha)]$ respectively in each pixel. The top axes give the resulting $E(B - V)$ from the balmer decrement assuming the O'Donnell (1994) Galactic extinction curve.

lating the Balmer decrement can be seen in figure 3 which shows the spread of the equivalent width based Balmer decrement ($\log[\text{EW}(\text{H}\alpha)/\text{EW}(\text{H}\beta)]$) against the “true” Balmer decrement determined from the stellar continuum-subtracted line fluxes ($\log(\text{H}\alpha/\text{H}\beta)$) for the SN($\text{H}\alpha, \text{H}\beta$) sample. Both the EW Balmer decrement and the flux Balmer decrement have been normalised to the intrinsic ratio of 2.86, appropriate for a low density gas of $T = 10^4$ K.

One of the first obvious issues to be corrected for is the variation of the underlying stellar continuum between the $\text{H}\alpha$ and $\text{H}\beta$ wavelengths. In the left diagram of figure 3, we show the distribution of $\log[\text{EW}(\text{H}\alpha)/\text{EW}(\text{H}\beta)]$, uncorrected for the continuum flux variation, while on the right the more accurate form of the EW Balmer decrement is used: $\log[\text{EW}(\text{H}\alpha)/\text{EW}(\text{H}\beta)] + \log[F_\lambda(\text{H}\alpha)/F_\lambda(\text{H}\beta)]$, where $F_\lambda(\text{H}\alpha)$ is the continuum flux at $\text{H}\alpha$, determined from a 200 pixel median smoothing of the emission-line subtracted continuum.

When uncorrected for the underlying continuum variation there is a clear systematic offset of the EW Balmer decrement from the 1:1 relation of ~ 0.1 dex. Correcting for the continuum variation removes this offset, yet a significant spread remains. This spread is due to the effect of the stellar Balmer absorption features. Without these, $\text{EW}(\text{H}\alpha) \times F_\lambda(\text{H}\alpha)$ should be, by definition, the flux of the line. The colors in figure 3a indicate the median $\text{H}\delta$ absorption index ($\text{H}\delta_{\text{Abs}}$, Worthey & Ottaviani 1997; Kauffmann et al. 2003a) of the sample in each pixel. As the figure shows, while the absolute strength of the stellar Balmer absorption features does play a part in the observed offset of the SDSS galaxies’ EW Balmer decrements, the dominant mechanism for the offset and spread is the *relative* strength of the stellar absorption features to the emission lines. This can be seen by the distribution of the equivalent width of the $\text{H}\alpha$ emission line indicated by the colours in figure 3b, where there is a clear gradient of decreasing $\text{EW}(\text{H}\alpha)$ with increasing offset from the line. As the emission lines become weaker overall, the stellar absorption features, which are $< 10\text{\AA}$ as discussed in section 2, obscure a greater fraction of $\text{H}\beta$ relative to $\text{H}\alpha$ and therefore lead to a larger offset.

As discussed in the introduction, the best way to compensate for the effect of the stellar absorption features on the emission lines

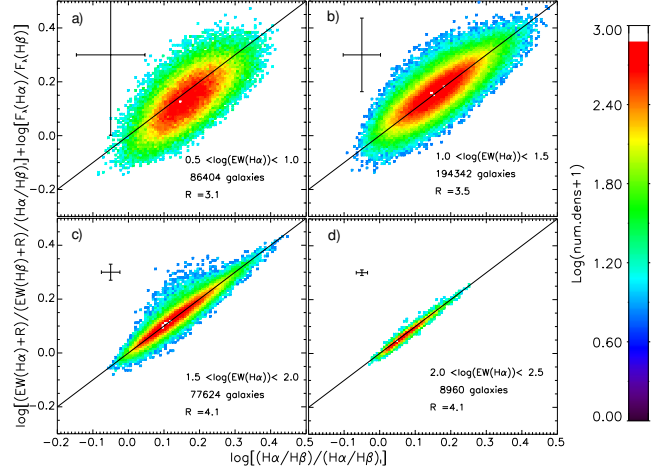


Figure 4. 2D histograms of the distribution of the SDSS SN($\text{H}\alpha, \text{H}\beta$) sample galaxies’ equivalent-width based Balmer decrements ($\log[\text{EW}(\text{H}\alpha)/\text{EW}(\text{H}\beta)]$), including a constant correction for stellar Balmer absorption, versus the stellar continuum-subtracted flux based Balmer decrements. Each figure shows a different bin of $\text{H}\alpha$ equivalent width, as labelled in lower right of each plot (in \AA). As in figure 3, both axes are normalized by the intrinsic Balmer ratio, $(\text{H}\alpha/\text{H}\beta)_I = 2.86$. The colours indicate the log of the number density in each pixel, as labelled by the colour bar on the right, with pixels with less than 5 galaxies excluded. The error bars in the upper left indicate the median uncertainty for each sample, with the total number of galaxies listed in the lower right of each plot. Note that the y-axis has a different correction for stellar Balmer absorption, R , for each plot as indicated in the lower left of each plot, and that galaxies with $\text{H}\beta$ still in absorption after correction (i.e. $\text{EW}(\text{H}\beta) + R < 0$) have been excluded from the sample.

is to fit the stellar continuum as done within the MPA/JHU SDSS database. However, when only poor quality spectra are available such as for high redshift galaxies, the determination of the Balmer absorption features may be unreliable. One possible approach when faced with low resolution spectra is to assume that the absorption equivalent width is constant for both Balmer lines across the whole sample. While figure 1 clearly shows that the absorption EW is *not* the same for all the Balmer lines, it provides a first step when information is sparse and uncertainties large. When a constant Balmer absorption correction R is assumed for both $\text{EW}(\text{H}\alpha)$ and $\text{EW}(\text{H}\beta)$, a correction factor of $R = 4\text{\AA}$ is determined when the offset of the SDSS galaxies’ EW Balmer decrements to the measured $\text{H}\alpha/\text{H}\beta$ ratios is minimized using an error-based weighting. The inclusion of this simple correction factor improves the situation when compared to that shown in figure 3, but with a still significant scatter of $\sigma \sim 0.1$ dex around the expected value and an extended tail of objects towards lower values. Both the scatter and the tail arise due to the assumption of a constant offset (i.e. Balmer absorption) for the whole sample. The value determined is biased towards high $\text{EW}(\text{H}\alpha)$ galaxies, as these galaxies both dominate the sample and have lower uncertainties, as discussed in section 3.

When split into bins of different $\text{EW}(\text{H}\alpha)$, more accurate fits with differing correction factors are obtained. In figure 4, we show the fits for the galaxies split into four bins; $0.5 < \log(\text{EW}(\text{H}\alpha)) < 1.0$, $1.0 < \log(\text{EW}(\text{H}\alpha)) < 1.5$, $1.5 < \log(\text{EW}(\text{H}\alpha)) < 2.0$, and $2.0 < \log(\text{EW}(\text{H}\alpha)) < 2.5$. The number of galaxies in each bin is listed in the lower right of each figure, and the median uncertainties are shown by the error bars in the upper left. Note that galaxies with $\text{H}\beta$ still in absorption after the correction factor R is applied have been excluded, but that this is less than 0.2% of the sample in each

bin. As can be seen in the figure, the median uncertainties increase quickly with decreasing emission line equivalent width. It is for this reason that galaxies with $\log(\text{EW}(\text{H}\alpha)) < 0.5$ have not been included here.

The y-axis for all four plots includes a correction for stellar absorption; $\log[(\text{EW}(\text{H}\alpha) + R)/(\text{EW}(\text{H}\beta) + R)] + \log[F_\lambda(\text{H}\alpha)/F_\lambda(\text{H}\beta)]$. As for the full sample, we determine the correction factor, R , for each binned sample by finding the value that leads to the minimum offset from the 1:1 relation with the uncertainties giving 1σ offsets from this relation. The values determined are $R = 3.1, 3.5, 4.1$, and 4.1\AA for each increasing bin of EW respectively, as indicated in the lower-left of each plot in figure 4. The 1σ uncertainty around R for each bin is approximately 1.0 (slightly less for the $\text{EW}(\text{H}\alpha) > 100\text{\AA}$ bin). The lowest bin has an uncertainty of 1.5, though the probability distribution for R is slightly skewed to higher values, arising from the offset visible in 4a, discussed below. The Balmer decrement determined from the EWs is significantly better than for the full sample, and especially so when no correction is included (figure 3), with dispersions of $1\sigma \sim 0.11, 0.06, 0.05$, and 0.04 dex around the 1:1 line respectively for the 4 binned samples.

The lowest $\text{EW}(\text{H}\alpha)$ (figure 4a) sample appears by eye to be slightly offset from the line. A reasonable hypothesis is that this offset arises due to our simple assumption of a constant correction R to both $\text{EW}(\text{H}\alpha)$ and $\text{EW}(\text{H}\beta)$, whereas it is clear from 1 that the absorption $\text{EW}(\text{H}\alpha)$ is typically less than the absorption EW of $\text{H}\beta$ by approximately a factor of 0.6 on average. However, changing the correction factor of $\text{EW}(\text{H}\alpha)$ to $0.6R$ and redoing the fit does not remove this offset. On closer examination it is clear that this offset is due to a biasing of the fit to the high signal-to-noise data, which predominantly occur at high values of the $\text{H}\alpha/\text{H}\beta$ ratio due to measurement biases (i.e. there is a clear gradient in $\text{EW}(\text{H}\alpha)$ from top to bottom in figure 4a). Assuming uniform weighting for the fit (i.e. ignoring the errors in EWs) gives a value of $R = 3.0$, well within the large uncertainties for R . For the other figures, assuming an offset correction factor for $\text{EW}(\text{H}\alpha)$ of $0.6R$, results in $R = 3.5, 3.7$, and 3.7\AA in terms of increasing EWs, with similar dispersion around the relations. The results are within the uncertainties for R when assuming a constant correction, but in all cases indicate the necessity for the correction of stellar absorption to the emission lines of a factor of $\sim 4\text{\AA}$.

For figures 4a, b, and d ($0.5 < \log(\text{EW}(\text{H}\alpha)) < 1.0$, $1.0 < \log(\text{EW}(\text{H}\alpha)) < 1.5$, and $2.0 < \log(\text{EW}(\text{H}\alpha)) < 2.5$ respectively) the observed scatter is less than the median uncertainty. Only for figure 4c does there appear to be a significant, low number scatter above the line (note the log scale density in figure 4). However, when examined, the scatter in this diagram, and also in figures 4a, b, and d, is correlated with the uncertainty in the determined $\text{H}\alpha$ and $\text{H}\beta$ lines, with the median scatter in each pixel increasing significantly the further from the line. Thus the median uncertainty for the outliers is greater than the median uncertainty of the sample as a whole in figure 4c.

While figure 4 demonstrates that it is possible to determine the Balmer decrement to some accuracy from emission line equivalent widths, the determination of the correction is dependent upon the measurement of three quantities; $\text{EW}(\text{H}\alpha)$, $\text{EW}(\text{H}\beta)$, and the flux ratio, $F_\lambda(\text{H}\alpha)/F_\lambda(\text{H}\beta)$. While the former two will be observable in strong emission line galaxies at high redshift, the flux ratio may prove problematic to measure from spectra. However this ratio is closely tied with the observed optical colours of the galaxy. In figure 5 we show the distribution of the continuum fluxes measured at the $\text{H}\alpha$ and $\text{H}\beta$ wavelengths ($F_\lambda(\text{H}\alpha)/F_\lambda(\text{H}\beta)$) against the restframe $g - r$ colour as measured from the SDSS fibre spectrum within the

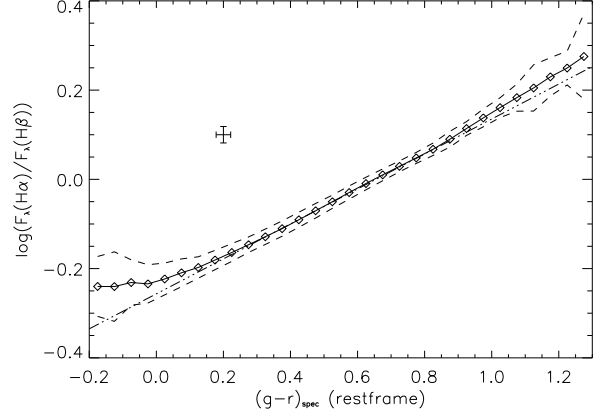


Figure 5. Distribution of the full $\text{SN}(\text{H}\alpha, \text{H}\beta)$ SDSS sample ratio of continuum fluxes measured at the $\text{H}\alpha$ and $\text{H}\beta$ wavelengths ($F_\lambda(\text{H}\alpha)/F_\lambda(\text{H}\beta)$) against the restframe $g-r$ colour as measured from the SDSS fibre spectrum. The solid line with diamonds shows the median $F_\lambda(\text{H}\alpha)/F_\lambda(\text{H}\beta)$, while the dashed lines show the 1σ dispersion. Median uncertainties are indicated by the error bars in the upper left. The thick dot-dot-dashed line indicates the best fit linear relation, with $y = -0.26 + 0.39(g - r)$.

full $\text{SN}(\text{H}\alpha, \text{H}\beta)$ sample. A linear fit to the correlation in this figure returns

$$\log(F_\lambda(\text{H}\alpha)/F_\lambda(\text{H}\beta)) = -0.26 + 0.39(g - r)_{\text{spec}}, \quad (1)$$

with a standard deviation of $\sigma \sim 0.015$ dex around this relation. We use the rest-frame $g - r$ colour as a proxy for stellar continuum, but other colours such as $r - i$ provide similar constraints. In the case of low-S/N spectra, the rest-frame colour could be from SED fitting to broad-band magnitudes.

Thus, in summary, the Balmer decrement for a low-resolution, strong-emission-line spectrum can be measured from the emission line equivalent widths and colours alone with;

$$\log(\text{H}\alpha/\text{H}\beta) = \log\left(\frac{\text{EW}(\text{H}\alpha) + 4.1}{\text{EW}(\text{H}\beta) + 4.1}\right) + (-0.26 + 0.39(g - r)_{\text{rest}}), \quad (2)$$

with a scatter around this of $\sigma \sim 0.05$ dex, or ~ 0.3 mag in A_V , assuming a Galactic extinction law (e.g. O'Donnell 1994). For weaker emission line galaxies (i.e. $\text{EW}(\text{H}\alpha) < 30\text{\AA}$), a lower offset ($R \sim 3.5$) should be used, as shown in figure 4. However, given the larger uncertainties and greater dispersion seen at lower $\text{EW}(\text{H}\alpha)$, a correction factor of $R \sim 4$ can be used for the full sample with a 0.1 dex scatter (~ 0.7 mag in A_V) and an extension to lower values (i.e. EW Balmer decrement underestimate) due to low EW systems.

One final note on this relation: as seen in figure 3, there is a strong bias in the sample of Balmer decrement with other galaxy properties, as discussed in detail in several other SDSS papers (see e.g. Kauffmann et al. 2003a; Garn & Best 2010). Thus, the relation shown above includes a combination of both galaxy type as well as variation in extinction. The only way to remove fully this effect is to match pairs of galaxies in as many property types excluding extinction, such as done in Wild et al. (2011b). Unfortunately when applied to the sample here, it was found that the range in extinction was not large enough to properly determine the relation. However, even given these uncertainties, this relation should still hold at several redshifts as high attenuations are on average associated with high gas masses, and thus high star formation rates and similar underlying continua at all redshifts.

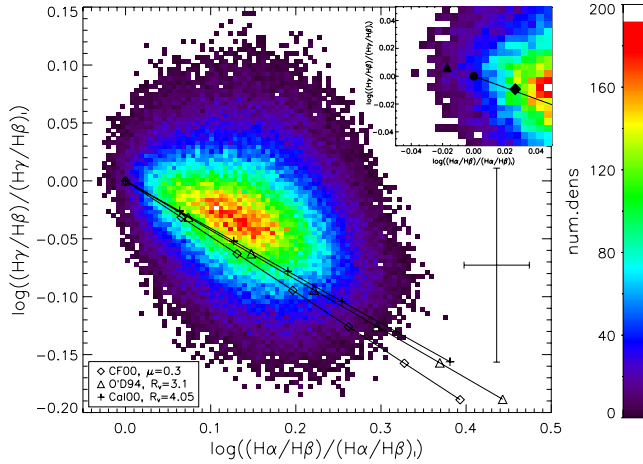


Figure 6. The distribution of $H\gamma/H\beta$ ratios versus $H\alpha/H\beta$ ratios for the SDSS SN($H\alpha, H\beta, H\gamma$) sample, with the number density of each pixel indicated by the bar on the right and pixels with less than 10 galaxies not shown. Both axes are normalised to their respective Case B ratios with $(H\alpha/H\beta)_I = 2.86$ and $(H\gamma/H\beta)_I = 0.468$. The median uncertainty of the sample is indicated by the error bars on the right. Overplotted are the variation expected from three different attenuation laws; Charlot & Fall (2000, CF00, diamonds), O’Donnell (1994, O’D94, triangles), and Calzetti et al. (2000, Cal00, plus signs) (see text). Each symbol represents a step of 0.5 in A_V , up to $A_V = 3$. *Inset:* A zoomed in version of the figure, showing the position of the zero point when the intrinsic ratios $((H\alpha/H\beta)_I$ and $(H\gamma/H\beta)_I$) are taken to be at $T=5,000K$ (diamond: 3.04, 0.458), at 10,000K (circle: 2.86, 0.468), and at 20,000K (triangle: 2.75, 0.475). The solid line shows the variation of the ratios with the Calzetti et al. (2000) attenuation law.

5 STELLAR ABSORPTION EFFECTS ON THE EMISSION LINES

One issue with the previous section is that we assume throughout that the stellar-continuum subtracted emission line fluxes within the MPA/JHU database are correct. While the overall fits to the stellar continuum are impressively good with a median $\chi^2 = 1.01$ per pixel across the sample, there are appear to be remaining issues around the Balmer lines. In the following we concentrate on the SDSS DR7 Balmer emission-line fluxes corrected for the underlying stellar absorption features from the MPA/JHU database, and explore their uncertainties using the known intrinsic values and commonly used attenuation and extinction laws.

5.1 The issue with $H\beta$

When considered alone, the ratio of $H\alpha/H\beta$ cannot indicate problems with the measurement of the lines involved unless it is significantly below the expected value of the unattenuated ratio. This is because the larger values of the emission line ratio can be caused by attenuation by intervening dust, with the intrinsic ratio dependent the emitting gas density and temperature (as discussed in section 2). However by examining several of the Balmer lines at once these dependencies can be accounted for.

Figure 6 shows the variation of the $H\gamma/H\beta$ ratio against the $H\alpha/H\beta$ ratio for the SN($H\alpha, H\beta, H\gamma$) SDSS sample. Both ratios have been normalized to their Case B, $T=10,000K$, $n_e = 100 \text{ cm}^{-3}$ intrinsic ratios $((H\alpha/H\beta)_I = 2.86, (H\gamma/H\beta)_I = 0.468)$. Immediately obvious in this figure is the offset of the sample from the zero point, indicating most SDSS galaxies undergo some attenuation (as seen

in the previous plots), with the correlation between the two ratios as expected from the reddening laws applied to the intrinsic ratio.

The three different lines overplotted show the effect of three different attenuation laws commonly assumed in the analysis of galaxies. For all three lines, the symbols indicates steps of 0.5 in A_V , up to $A_V = 3$.

The O’Donnell (1994) law (O’D94) is an updated version of the Cardelli et al. (1989) fit to the average extinction law in the Galaxy, thus least representative of the integrated emission from the SDSS galaxies, which will suffer attenuation due to the mixture of emitting sources and absorbing medium. However, as discussed in Kennicutt et al. (2009) and can be seen in figure 6, the use of a foreground dust screen with galactic extinction is indistinguishable from the other laws, especially given the uncertainty within the SDSS sample. We assume a total to selective V -band extinction of $R_V = 3.1$, the average value in our galaxy.

The Calzetti et al. (2000) attenuation law (Cal00) was obtained from the continuum and Balmer decrement of local actively star-forming galaxies, thus matching the high $EW(H\alpha)$ galaxies in the sample. Note that as only ratios are analysed here, the difference between the colour excess ($E(B - V)$) of the stellar continuum and nebular lines noted by Calzetti et al. is effectively scaled out. The R_V used here is 4.05, as given by Calzetti et al. (2000) from the comparison of the observed infrared flux to that predicted from the obscuration of the optical-ultraviolet light.

The Charlot & Fall (2000) attenuation law (CF00) is a more simple, empirical law put forward to allow for the different colour excesses and attenuations observed by Calzetti et al. (2000) between the nebular emission lines and stellar continuum. It breaks the attenuation into two components; the ‘diffuse ISM’ component that describes the effective obscuration of all stars in a galaxy by the diffuse dust, and the ‘birth cloud’ component that describes the additional extinction suffered by the $H II$ regions from which the nebular emission lines arise, giving

$$\frac{A_\lambda}{A_V} = \mu(\lambda/\lambda_V)^{-0.7} + (1 - \mu)(\lambda/\lambda_V)^{-1.3}, \quad (3)$$

where $\lambda_V = 5500\text{\AA}$. The exponent of -0.7 for the diffuse ISM was empirically derived by Charlot & Fall (2000) with a comparison of nearby galaxies, while the -1.3 exponent for the birth clouds was chosen to match the extinction within our own Galaxy. The parameter μ indicates the fraction of the attenuation suffered by the nebular lines by each component. We assume $\mu = 0.3$ here, as used by Wild et al. (2007) and Wild et al. (2011a) in their analyses of SDSS galaxies.

There are three things of note to take from figure 6: One, given enough precision in the data, the SDSS galaxies should be able to distinguish between these three different attenuation laws, and provide an answer on which law is best (or least bad) to apply to an ensemble of galaxies. Such work has been done before for comparing galactic extinction laws using planetary nebulae (Phillips 2007). Note that the different R_V between the Cal00 and O’D94 laws is what causes the difference in expected $H\alpha/H\beta$ for the same A_V , while the CF00 and Cal00 have similar A_V as determined from $H\alpha/H\beta$, but not from $H\gamma/H\beta$. Two, that the scatter of the SDSS galaxies is large around the three laws, preventing this possibility, though this scatter is not significant when compared to the median uncertainty as shown by the error bars. Third, and most importantly, while the slope of SDSS galaxies matches that given by the attenuation laws, *there is a systematic offset of the SDSS galaxies when compared to all three attenuation laws*. This offset is significant, and cannot be explained by assuming more extreme (and therefore

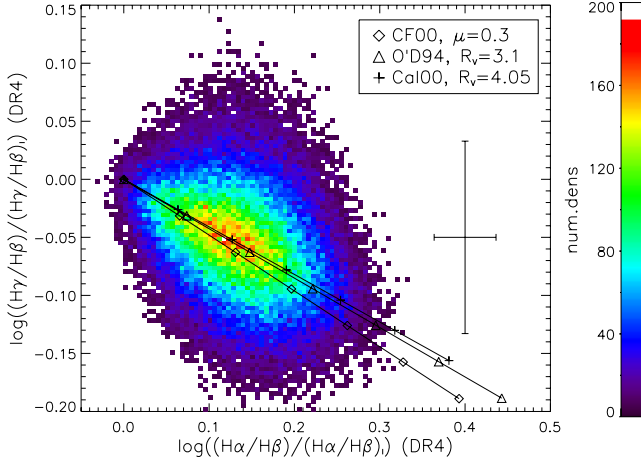


Figure 7. The same plot as figure 6, except using the SDSS DR4 MPA/JHU catalogue. The same SN cuts on $H\alpha$, $H\beta$, and $H\gamma$ are applied, with $\sim 160,000$ galaxies in the sample.

less likely) attenuation laws or by assuming large values of R_V , as the zero point itself appears to be offset.

Neither can this situation be remedied by assuming different values for the unattenuated Balmer ratios. As discussed in section 2, the intrinsic Balmer emission-line ratios are sensitive to the temperature of the ionized gas from which they arise, and, more weakly, to the density of the gas as well. The inset in figure 6 shows a close up of the zero point of figure 6, i.e. galaxies with little or no attenuation. Over this are plotted 3 symbols indicating the position where the zero point would be for 3 different average $H II$ region temperatures; 5,000K, 10,000K (assumed within the figure), and 20,000K. All assume Case B ratios, and a typical $H II$ gas density of $n_e = 10^2 \text{ cm}^{-3}$. These 3 temperatures encompass the range of temperatures expected, with typical solar metallicity $H II$ regions having $T_e \sim 8,000\text{K}$. What this figure demonstrates is that the variation in intrinsic Balmer ratios is small relative to both the effects of attenuation and the observed offset, and that the variation in intrinsic ratios is in the same sense as that due to the effects of attenuation (as shown by the Calzetti et al. (2000) law), thus the intrinsic ratio cannot be the cause of the offset.

A possible cause for this offset can be found when the MPA/JHU DR4 catalogue is examined instead. Using the same SN cuts on $H\alpha$, $H\beta$, and $H\gamma$, figure 7 shows the same plot as figure 6 for the DR4 sample. In most ways this figure is exactly the same (as it should be), except in two respects: the DR4 SN($H\alpha, H\beta, H\gamma$) sample only has $\sim 160,000$ galaxies in the sample compared to the $\sim 240,000$ galaxies in the DR7 sample, visible in both the number density (colours) and in the scatter, and the DR4 sample does not have the offset with respect to the attenuation laws seen in figure 6.

As mentioned in section 3, the major difference between the DR4 and DR7 line fluxes from the MPA/JHU catalogues is the version of the GALAXEV models used for the continuum fits. In some respects the difference seen in the figures is surprising, as the median χ^2 of the fits to the continuum in DR7 is reduced compared to the DR4 fits, from $\chi^2 = 1.5$ for DR4 to $\chi^2 = 1$ for DR7, suggesting a much better fit to the spectra.

The issue most likely lies within the $H\beta$ line region, as an offset in the $H\beta$ line flux would also explain the increasing offset at higher $(H\alpha/H\beta)$ between the SDSS galaxies and the attenuation laws, and this region has been observed to be mismatched between models and the spectra of some globular clusters (see e.g.

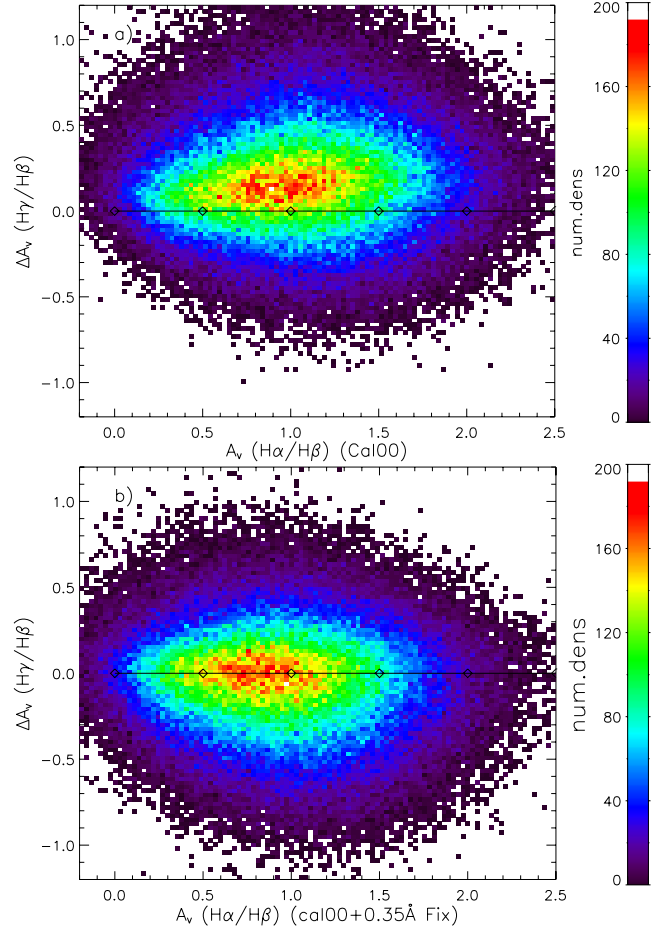


Figure 8. **a)** The same diagram as Figure 6, but rotated to A_V axes using the attenuation law of Calzetti et al. (2000). The x -axis is the A_V as measured from the $(H\alpha/H\beta)$ ratio, while the y -axis is the offset from the expected $(H\gamma/H\beta)$ ratio based on this A_V . **b)** The same as **a)**, but the $H\beta$ line flux has been corrected for under subtraction of the stellar continuum by 0.35\AA .

Walcher et al. 2009; Poole et al. 2010). This difference in slope is more clearly seen in figure 8a where we have rotated and scaled figure 6 to the A_V plane using the attenuation law of Calzetti et al. (2000), where the offset from the x -axis is more clearly seen. Similar results are seen if another attenuation law is used. In this frame, the y -axis is the offset from the expected $(H\gamma/H\beta)$ ratio based on the A_V as determined by the $(H\alpha/H\beta)$ ratio.

By “correcting” for the incorrectly subtracted stellar $H\beta$ equivalent width we can fix figure 8a. This is what we have done in figure 8b, where we have added 0.35\AA to the emission line equivalent width (i.e. “True” $H\beta = H\beta + 0.35F_\lambda(H\beta)$). The correction of 0.35\AA was determined by minimizing the offset from the Calzetti law (this value depends only weakly on the choice of attenuation law). This means that the stellar absorption equivalent width of $H\beta$ is systematically underestimated by 0.35\AA in the CB08 continuum fits to DR7 SDSS spectra.

The fact that this 0.35\AA underestimation is systematic is interesting, as we would expect that any error would depend on the strength of the Balmer features, either measured through the $H\delta_{\text{Abs}}$ or the emission line equivalent widths, both of which do correlate with $H\alpha/H\beta$ as seen in figure 3, yet no correlation is observed. What the underlying cause of this systematic underestimation is unknown, yet it must be taken into consideration when determin-

ing the A_V from the Balmer decrement in the SDSS DR7 MPA/JHU catalogue. It is possible that this issue arises due to the misclassification of the spectral resolution of the MILES library (as discussed in Falcón-Barroso et al. 2011) in the implementation in the CB08 code, but this issue is now known and currently under investigation. This investigation goes beyond the scope of the work presented here but we note that the models used here are early versions of the CB08 library and these issues are expected to be solved within the to-be-published models. When the new A_V is calculated from the $H\alpha/H\beta$ ratio including the systematic 0.35\AA offset (using e.g. Calzetti et al. 2000, law), a mean difference of -0.07 magnitudes is found with the uncorrected A_V estimates, increasing slightly at higher A_V . This suggests that previous DR7 A_V estimates, such as in Garn & Best (2010), are overestimated by this value.

Similarly this 0.35\AA correction must be included in our EW Balmer decrement (equation 2) leading to a new equation,

$$\log(H\alpha/H\beta) = \log\left(\frac{EW(H\alpha) + 4.1}{EW(H\beta) + 4.4}\right) + (-0.26 + 0.39(g - r)_{\text{rest}}), \quad (4)$$

which more closely matches our expectations of different stellar absorption equivalent widths between $H\alpha$ and $H\beta$. For weaker emission line galaxies, the offset would be smaller than 4.1, as shown in figure 4 and discussed at the end of section 4.

5.2 The issue with $H\delta$

While examining the issue in $H\beta$, a similar issue was found for $H\delta$ that we present here as a curiosity. When $H\delta/H\alpha$ versus $H\gamma/H\alpha$ is plotted, using the SN($H\alpha, H\beta, H\gamma, H\delta$) sample of SDSS galaxies and avoiding the problematic $H\beta$ line, the tight correlation between these two ratios, matching closely that expected from the attenuation by dust. However, upon closer examination, a systematic offset is observed between the galaxies and attenuation laws. As in the previous subsection on $H\beta$, the offset is clearer when rotated to the A_V plane, which is what we show in figure 9, where the x -axis is the A_V determined from $H\gamma/H\alpha$ using the Calzetti et al. (2000) law, with the y -axis the offset from this A_V when determined from the $H\delta/H\alpha$ ratio. The median offset is ~ -0.05 for most of the A_V range shown here, meaning that the A_V determined from $H\delta/H\alpha$ is lower than that determined from $H\gamma/H\alpha$. The offset is seen for all attenuation laws considered here.

More importantly, the offset is also observed in the DR4 sample, though with greater uncertainty due to low number statistics. As with the $H\beta$ line there appears to be no correlation of the offset with emission line equivalent widths, or stellar age determinants like $H\delta_{\text{Abs}}$ or the D_n4000 index (see Kauffmann et al. 2003a, for definitions of these indices). Neither does it appear to be correlated with $H\alpha/H\beta$ or other emission line or attenuation tracers. Thus, due to the lack of difference between DR4 and DR7, the strong EW bias of the sample (as shown in figure 2), and the fact that the uncertainty is dominated by the $H\delta$ line, it is still not known what exactly causes this offset. It is most likely an issue due to the underlying continuum, but an investigation into the stellar models goes beyond the scope of this work. Thus we present this issue for now as a curiosity and a cautionary note of the level of systematic uncertainties in determining weak line fluxes from the SDSS sample.

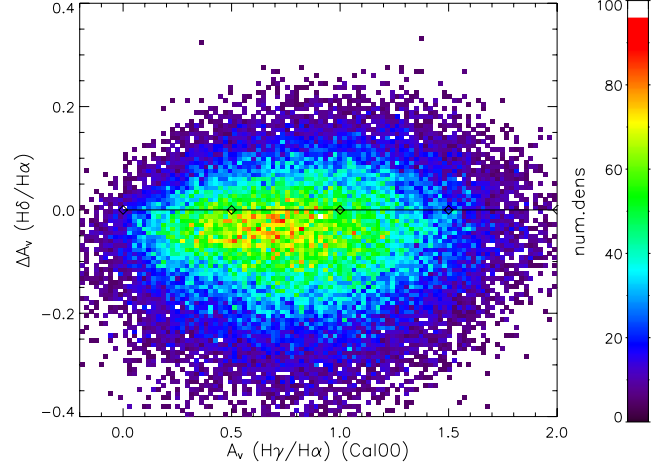


Figure 9. The distribution of $H\delta/H\alpha$ versus $H\gamma/H\alpha$ for the SN($H\alpha, H\beta, H\gamma, H\delta$) sample of SDSS DR7 galaxies ($\sim 121,00$ objects). As in figure 8, the figure is rotated and scaled to the A_V plane as determined from the Calzetti et al. (2000) law, indicated by the straight line. The number of galaxies in each pixel is indicated by colours (as labelled), with pixels with less than 5 galaxies not shown.

6 CONCLUSION

We have examined the possibility of using equivalent widths of the Balmer emission lines to determine the Balmer decrement, and hence attenuation, of a galaxy. Using the Sloan Digital Sky Survey we were able to determine a statistically representative relation between the continuum-subtracted Balmer emission line flux ratio and the equivalent widths (EW) of the Balmer emission-lines combined with a rest-frame colour, correcting for the effects of the stellar absorption features:

$$\log(H\alpha/H\beta) = \log\left(\frac{EW(H\alpha) + 4.1}{EW(H\beta) + 4.4}\right) + (-0.26 + 0.39(g - r)), \quad (5)$$

for galaxies with $EW(H\alpha) \gtrsim 30\text{\AA}$, with a scatter of $1\sigma \sim 0.06$ dex, or 0.4 mag in A_V , indicating the possible variation for individual objects. For galaxies with $EW(H\alpha) < 30\text{\AA}$ smaller correction factors (3.5 for $EW(H\alpha)$, 3.8 for $EW(H\beta)$) should be used. However, given the scatter at low EW values, the equation above can be used above for all galaxies allowing for a much greater uncertainty in the final Balmer ratio or A_V determined.

In addition, by comparing the Balmer decrement ($H\alpha/H\beta$ versus $H\gamma/H\beta$) we discovered that the $H\beta$ emission line equivalent width (and hence flux) is underestimated by 0.35\AA in the JHU/MPA DR7 SDSS database, due to an issue in the $H\beta$ region of the 2008 version of the Charlot & Bruzual stellar population synthesis code GALEXEV. This leads to an overestimation of the attenuation of the SDSS galaxies of 0.07 magnitudes in A_V assuming a Calzetti et al. (2000) attenuation law.

Finally, we also discovered a strange offset in the $H\delta$ emission line fluxes observable in both the DR4 and DR7 releases of the MPA/JHU database which we present both as a curiosity and as a warning on the underlying issues in interpreting weak-line emission lines in a statistical sample

ACKNOWLEDGEMENTS

BG would like to thank V. Wild for providing her PCA principal component values available and very helpful discussions, and the authors would like to thank the referee for helpful comments.

Funding for the SDSS and SDSS-II has been provided by the Alfred P. Sloan Foundation, the Participating Institutions, the National Science Foundation, the U.S. Department of Energy, the National Aeronautics and Space Administration, the Japanese Monbukagakusho, the Max Planck Society, and the Higher Education Funding Council for England. The SDSS Web Site is <http://www.sdss.org/>.

The SDSS is managed by the Astrophysical Research Consortium for the Participating Institutions. The Participating Institutions are the American Museum of Natural History, Astrophysical Institute Potsdam, University of Basel, University of Cambridge, Case Western Reserve University, University of Chicago, Drexel University, Fermilab, the Institute for Advanced Study, the Japan Participation Group, Johns Hopkins University, the Joint Institute for Nuclear Astrophysics, the Kavli Institute for Particle Astrophysics and Cosmology, the Korean Scientist Group, the Chinese Academy of Sciences (LAMOST), Los Alamos National Laboratory, the Max-Planck-Institute for Astronomy (MPIA), the Max-Planck-Institute for Astrophysics (MPA), New Mexico State University, Ohio State University, University of Pittsburgh, University of Portsmouth, Princeton University, the United States Naval Observatory, and the University of Washington.

REFERENCES

- Abazajian, K. N., et al. 2009, *ApJS*, 182, 543
- Adelman-McCarthy, J. K., et al. 2006, *ApJS*, 162, 38
- Baker, J. G., & Menzel, D. H. 1938, *ApJ*, 88, 52
- Berman, L. 1936, *MNRAS*, 96, 890
- Brinchmann, J., Charlot, S., White, S. D. M., Tremonti, C., Kauffmann, G., Heckman, T., & Brinkmann, J. 2004, *MNRAS*, 351, 1151
- Bruzual, G., & Charlot, S. 2003, *MNRAS*, 344, 1000
- Calzetti, D., Armus, L., Bohlin, R. C., Kinney, A. L., Koornneef, J., & Storchi-Bergmann, T. 2000, *ApJ*, 533, 682
- Calzetti, D. 2001, *PASP*, 113, 1449
- Cappellari, M., & Emsellem, E. 2004, *PASP*, 116, 138
- Cardelli, J. A., Clayton, G. C., & Mathis, J. S. 1989, *ApJ*, 345, 245
- Cenarro, A. J., et al. 2007, *MNRAS*, 374, 664
- Charlot, S., & Fall, S. M. 2000, *ApJ*, 539, 718
- Cid Fernandes, R., Mateus, A., Sodré, L., Stasińska, G., & Gomes, J. M. 2005, *MNRAS*, 358, 363
- da Cunha, E., Eminian, C., Charlot, S., & Blaizot, J. 2010, *MNRAS*, 403, 1894
- Dopita, M. A., & Sutherland, R. S. 2003, *Astrophysics of the diffuse universe*, Berlin, New York: Springer, 2003. Astronomy and astrophysics library, ISBN 3540433627
- Falcón-Barroso, J., Sánchez-Blázquez, P., Vazdekis, A., Ricciardelli, E., Cardiel, N., Cenarro, A. J., Gorgas, J., & Peletier, R. F. 2011, *A&A*, 532, A95
- Ferland, G. J. 1999, *PASP*, 111, 1524
- Ferland, G. J., Fabian, A. C., Hatch, N. A., Johnstone, R. M., Porter, R. L., van Hoof, P. A. M., & Williams, R. J. R. 2009, *MNRAS*, 392, 1475
- Ferland, G. J., Korista, K. T., Verner, D. A., Ferguson, J. W., Kingdon, J. B., & Verner, E. M. 1998, *PASP*, 110, 761
- Gallazzi, A., Charlot, S., Brinchmann, J., White, S. D. M., & Tremonti, C. A. 2005, *MNRAS*, 362, 41
- Garn, T., & Best, P. 2010, *arXiv:1007.1145*
- Groves, B. A., Dopita, M. A., & Sutherland, R. S. 2004, *ApJS*, 153, 9
- González Delgado, R. M., & Leitherer, C. 1999, *ApJS*, 125, 479
- González Delgado, R. M., Leitherer, C., & Heckman, T. M. 1999, *ApJS*, 125, 489
- Kauffmann, G., et al. 2003, *MNRAS*, 341, 33
- Kauffmann, G., et al. 2003, *MNRAS*, 346, 1055
- Kennicutt, R. C., Jr., et al. 2009, *ApJ*, 703, 1672
- Kewley, L. J., Jansen, R. A., & Geller, M. J. 2005, *PASP*, 117, 227
- Kewley, L. J., Groves, B., Kauffmann, G., & Heckman, T. 2006, *MNRAS*, 372, 961
- Lamareille, F., Contini, T., Le Borgne, J.-F., Brinchmann, J., Charlot, S., & Richard, J. 2006, *A&A*, 448, 893
- Le Borgne, J.-F., et al. 2003, *A&A*, 402, 433
- Liang, Y. C., Hammer, F., Flores, H., Gruel, N., & Assémat, F. 2004, *A&A*, 417, 905
- Luridiana, V., Simón-Díaz, S., Cerviño, M., González Delgado, R. M., Porter, R. L., & Ferland, G. J. 2009, *ApJ*, 691, 1712
- Menzel, D. H., & Baker, J. G. 1937, *ApJ*, 86, 70
- Ocvirk, P., Pichon, C., Lançon, A., & Thiébaud, E. 2006, *MNRAS*, 365, 74
- O'Donnell, J. E. 1994, *ApJ*, 422, 158
- Osterbrock, D. E., & Ferland, G. J. 2006, *Astrophysics of gaseous nebulae and active galactic nuclei*, 2nd. ed. by D.E. Osterbrock and G.J. Ferland. Sausalito, CA: University Science Books, 2006
- Phillips, J. P. 2007, *New A*, 12, 378
- Poole, V., Worthey, G., Lee, H.-c., & Serven, J. 2010, *AJ*, 139, 809
- Sánchez-Blázquez, P., et al. 2006, *MNRAS*, 371, 703
- Seaton, M. J. 1959, *MNRAS*, 119, 90
- Storey, P. J., & Hummer, D. G. 1995, *MNRAS*, 272, 41
- Tojeiro, R., Heavens, A. F., Jimenez, R., & Panter, B. 2007, *MNRAS*, 381, 1252
- Tremonti, C. A., et al. 2004, *ApJ*, 613, 898
- Walcher, C. J., Coelho, P., Gallazzi, A., & Charlot, S. 2009, *MNRAS*, 398, L44
- Wild, V., Kauffmann, G., Heckman, T., Charlot, S., Lemson, G., Brinchmann, J., Reichard, T., & Pasquali, A. 2007, *MNRAS*, 381, 543
- Wild, V., et al. 2011, *MNRAS*, 410, 1593
- Wild, V., Charlot, S., Brinchmann, J., Heckman, T., Vince, O., Pacifici, C., & Chevallard, J. 2011, *arXiv:1106.1646*
- Worthey, G., & Ottaviani, D. L. 1997, *ApJS*, 111, 377